

THEORY AND EXPERIMENT OF A COMPACT WAVEGUIDE DUAL CIRCULAR POLARIZER

C. Chang^{1, 2, *}, S. Church^{2, 3}, S. Tantawi^{1, 2}, P. Voll^{2, 3},
M. Sieth^{2, 3}, and K. Devaraj^{2, 3}

¹SLAC National Accelerator Laboratory, Stanford University, Stanford, CA 94309, USA

²Kavli Institute for Particle Astrophysics & Cosmology, Stanford University, Stanford, CA 94309, USA

³Department of Physics, Stanford University, 382 Via Pueblo Mall, Stanford, CA 94305, USA

Abstract—A new compact and wide-band waveguide dual circular polarizer at Ka-band is presented and tested in this paper. This compact structure is composed of a three-port polarizing diplexer and a circular polarizer realized by a simple pair of large grooves. The polarizing diplexer includes two rectangular waveguides with a perpendicular H -plane junction, one circular waveguide coupled in E -plane. A cylindrical step and two pins are used to match this structure. For a LHCP or RHCP wave in the circular port, only one specific rectangular port outputs power and the other one is isolated. The accurate analysis and design of the circular polarizer are conducted by using full-wave electromagnetic simulation tools. The optimized dual circular polarizer has the advantage of compact size with a volume smaller than $1.5\lambda^3$, broad bandwidth, uncomplicated structure, and is especially suitable for use at high frequencies such as Ka-band and above. The prototype of the polarizer has been manufactured and test, the experimental results are basically consistent with the theories.

1. INTRODUCTION

In this paper, we develop a compact broadband waveguide dual circular polarizer. The design is intended for large-format focal plane arrays, which could be used in the next generation of cosmic

Received 26 July 2012, Accepted 29 August 2012, Scheduled 9 September 2012

* Corresponding author: Chao Chang (chang@slac.stanford.edu).

microwave background (CMB) polarization experiments to understand the very early Universe [1, 2]. The detected B-mode polarization is from Ka band to W band, which is received by the antenna array of circular feed horns. There are hundreds of units in the antenna array, thus each unit should be as compact as possible, wideband, and straightforward to mass-produce. The right hand and left hand circular polarized component (RHCP and LHCP) of the B-mode $Q \pm iU$ include important information, Q and U need to be amplified synchronously rather than separately, thus, before the amplifiers, dual circular polarizer is used to separate the circular polarized $Q \pm iU$ in two ports with linear polarizations (LP), one of which contains the information of $Q + iU$, and the other is for $Q - iU$.

The circular polarizer is usually designed to convert one linearly polarized mode into two orthogonal modes with a 90-degree phase shift by loading the discontinuities of septum [3–5], corrugations [6–9], dielectrics [10, 11]. The waveguide septum polarizer has the advantage of compact size with three physical ports, but has a very limited bandwidth due to phase shift of two orthogonal modes [12]; the dielectric-loaded polarizer has relative high loss. The polarizer for corrugations, dielectrics, and ridges are two physical ports, and need ortho-mode transducer (OMT) to separate the LHCP and RHCP. The Boifot OMT [13] has broad bandwidth but with very complex matching structure. There are four physical rectangular ports for turnstile OMT [14–16], which need two waveguide rings to respectively combine the ports with same polarization. Thus, turnstile OMT is not compact and the two waveguide rings may decrease the final bandwidth. The compact three-port branching OMT [17] composed by two H -plane rectangular waveguides coupled with a common circular waveguide uses two bottle-neck-like irises to match the structure and realize the isolation, whose return loss < -10 dB had a bandwidth $< 12\%$, and isolation < -35 dB with a bandwidth $> 10\%$. Other kind of circular polarizers such as microstrip polarizer [18–24] also have the disadvantage of narrow bandwidth and low efficiency due to losses of conductor, dielectric and surface wave.

As we mentioned above, since there are hundreds of units in the antenna array for detecting CMB, the dual circular polarizer should have compact size and broad bandwidth, which are the design goal in this paper. We focus on the Ka-band with frequency from 26 GHz to 36 GHz. Firstly, we design and optimize a compact 3 physical-port polarizing diplexer which can separate the circular polarized wave $Q \pm iU$ from a circular port into two separate rectangular ports with linear polarized Q and $\pm iU$. Then, two symmetric grooves are used to form the circular polarizer.

2. THE DESIGN OF THE COMPACT POLARIZING DIPLEXER

The compact three physical-port polarizing diplexer illustrated in Fig. 1 includes two rectangular waveguides with a perpendicular H -plane junction and one circular waveguide coupled in E -plane. This device contains a symmetric diagonal plane, called AA , which decomposes the structure into two equal halves. Because of the symmetry of the structure about AA , the full structure can be optimized by solving just one of the halves. The plane AA is defined to be the XZ plane in 3-dimensional Cartesian coordinates.

When the rectangular port 1 or 3 feeds in a TE_{10} mode, a specific TE_{11} mode polarized along the incident rectangular waveguide is generated, which can be further decomposed along the X and Y axes. In other words, for a TE_{10} mode inserted in port 1, two orthogonal TE_{11} modes with phase difference 0° respectively along X and Y axes are excited, compared with two TE_{11} modes with phase difference 180° for incident TE_{10} mode from port 3.

Optimization variables are used to define a central rectangular step as well as one pin on this step and located at the strong electric field region in the $1/2$ structure. Full-wave electromagnetic simulation HFSS software [25] is used to optimize the structure. In order to realize the whole structure matched, no matter for the symmetric plane AA is electric or magnetic boundary, there should be a broad band result for the $1/2$ structure. First of all, AA plane is assumed to be a perfect electric boundary, as shown in Fig. 2(a), and the parameters of the step and one pin are optimized. Then, AA is assumed to be a perfect magnetic boundary, as illustrated in Fig. 2(b), and another pin at the bottom of the waveguide is added in the strong magnetic region which

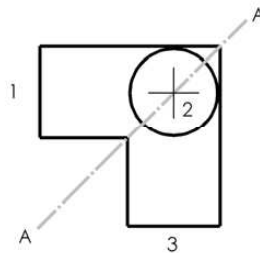


Figure 1. Schematic of the symmetric 3-port polarizing diplexer; Port 1, Port 2 and Port 3 are defined as illustrated.

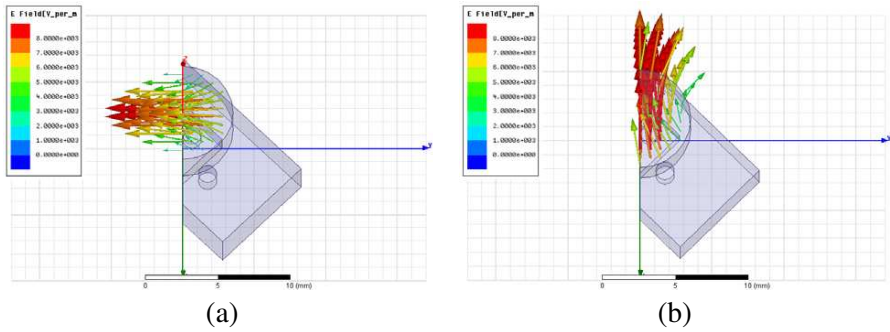


Figure 2. Electric field vector distribution for the symmetric diagonal plane as (a) a perfect electric wall and (b) a perfect magnetic wall; The frequency is 31 GHz.

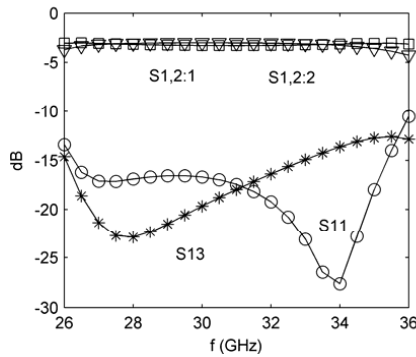
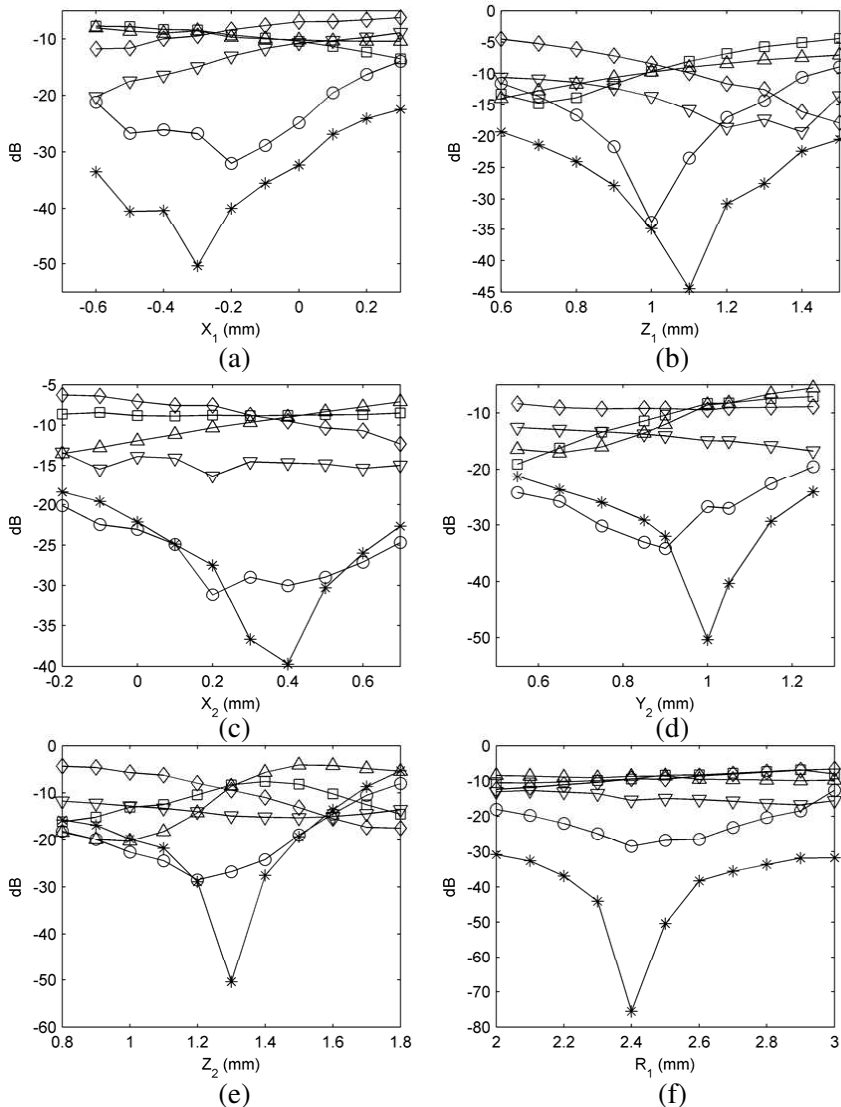


Figure 3. Optimized S -parameters for structure with four pins; 2 : 1 represents Port 2: mode 1, and 2 : 2 represents Port 2: mode 2.

is far away from the strong electric field region. Consequently, the second pin should have a weak influence on the optimized result for AA as an electric boundary.

It is found that the four pins structure is very difficult to optimize since there are too many parameters to consider, and the optimized S_{11} and S_{13} is about from -10 dB to -25 dB within the target bandwidth, as shown in Fig. 3. Thus, we use a circular step instead of the rectangular one and the four pins are replaced by two. Then, the key parameters for matching the structure are the radius R_1 and the height Z_1 of the step, the center position X_1 of the step and the circular waveguide, the radius R_2 , height Z_2 and the location X_2 and Y_2 of the pins.

The optimization module of HFSS software has a strong ability in matching a structure at a single frequency, but is not ideal for optimizing over a large bandwidth. Thus, the influence of the step and pins on the S parameters within the bandwidth is investigated by sweeping the parameters of the structure, while the S parameters at the central frequency (31 GHz) and the edge frequencies (26 GHz and 36 GHz) are monitored. The sweep results for each variable are plotted in separate graphs in Fig. 4.



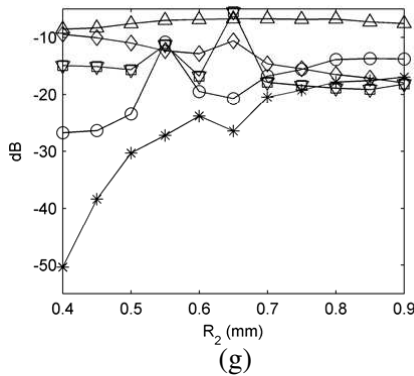


Figure 4. Variation of the S parameters with the parameters of (a) X_1 , (b) Z_1 , (c) X_2 , (d) Y_2 , (e) Z_2 , (f) R_1 and (g) R_2 , the data of symbol \bigcirc , \triangle , \square represent for S_{11} at 31 GHz, 26 GHz, and 36 GHz, and $*$, \diamond , and ∇ for S_{13} at 31 GHz, 26 GHz, and 36 GHz.

It is shown in Fig. 4(a) when the center position X_1 of the step and the circular waveguide deviates a little from the coordinate center and moves along the X -axis to the range $X_1 \sim -0.2$ to -0.4 mm, the return loss and isolation are significantly decreased. Additionally, when the radius of the step is $R_1 \sim 2.4$ – 2.5 mm and the height is 0.9 – 1.2 mm, both S_{11} and S_{13} are small. The structure is matched well when the pins deviate a little from the center of the step with $X_2 \sim 0.2$ – 0.4 mm the central distance between the two pins reaches $2Y_2 \sim 2 * (0.9 - 1)$ mm, and the height is $Z_2 \sim 1.2$ – 1.4 mm. Finally, a smaller R_2 has a higher isolation. It should be emphasized that taking the coordinate satisfying the symmetric plane AA to be the YZ plane was very important for calculating the optimization results.

Besides, the optimized broadband structure should keep S_{11} and S_{13} at the boundary frequencies 26 GHz and 36 GHz as low as possible. After sweeping the above multi-parameters of the pins and the step, the researched range of the variables for a matched structure could become smaller. The structure and the optimized S -parameters for the compact broadband polarizing diplexer is shown in Figs. 5(a) and (b). Compared with Fig. 3, the S parameters of the new structure in Fig. 5 have much lower return loss and higher isolation. The modes 1 and 2 in port 2 have 0 or 180° phase difference.

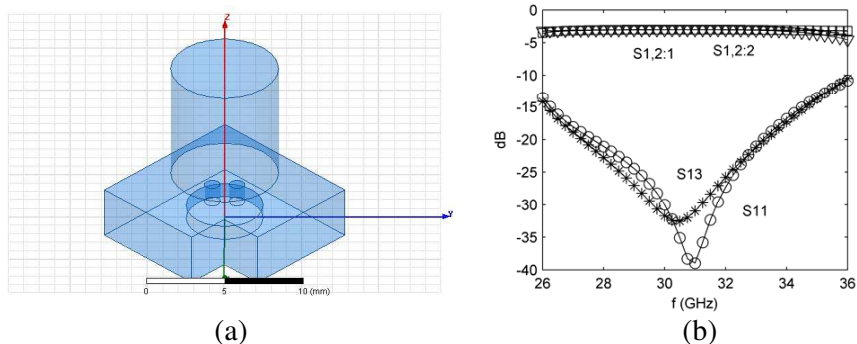


Figure 5. (a) The final structure of 3-port compact polarizing diplexer and (b) the optimized S parameter.

3. THE DESIGN OF THE DUAL CIRCULAR POLARIZER

A pair of grooves along the symmetric plane AA are used to adjust the phase difference $\Delta\varphi$ of the two orthogonal modes reaching 90° and keep the broadband result. A polarizer with single groove in Ref. [7] was researched. To keep the symmetric of the polarizer in this paper, a pair of large grooves are adopted, which can realized a broad bandwidth because it excites higher order modes, and weakens the frequency dependence of the phase variation βL , where L is the length of the groove and β is the propagation constant. For instance with a depth 2.5 mm and width 1.5 mm, a length $L \sim \lambda$ is needed to realize $\Delta\varphi \sim 90^\circ$, smaller grooves, with depth 1 mm and width 1 mm, would need a length of $L \sim 3\lambda$ to reach $\Delta\varphi \sim 90^\circ$ at 31 GHz and the dependence of $\Delta\varphi$ on frequency is very sensitive due to a larger phase variation $\Delta\beta L$ compared with a shorter L . By sweeping the height, width, and length of the grooves, the optimized parameters are illustrated in Fig. 6.

The results in Fig. 6 show that the return loss and isolation between the rectangular ports is below -10 dB and the phase differences of the two orthogonal TE_{11} modes maintains in the vicinity of 90° within a bandwidth of about 30%, the detailed parameters of the polarizer is shown in Table 1. From Fig. 7, the isolation between the two orthogonal TE_{11} modes is lower -40 dB, and the TE_{11} power is equally divided between Port 1 and Port 3, i.e., $S(2 : 1, 1) = S(2 : 2, 1) = S(2 : 1, 3) = S(2 : 2, 1) = -3$ dB. For the same phase of two TE_{11} modes, there are respectively 90° and -90° phase differences

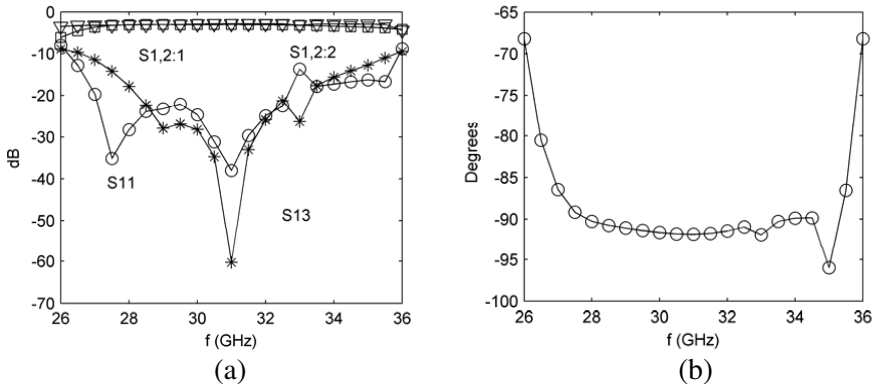


Figure 6. (a) The optimized S parameters and (b) the phase differences of the two orthogonal TE_{11} modes of the circular polarizer at Port 1.

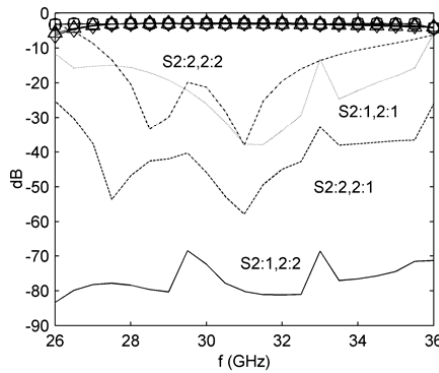


Figure 7. The optimized S parameters of the circular polarizer with regard to Port 2 (the solid line $S(2 : 1, 2 : 2)$, the dashed blue $S(S(2 : 2, 2 : 1))$, the dashed-dotted line $S(S(2 : 2, 2 : 2))$, the dotted line $S(2 : 1, 2 : 1)$, the diamond, circular, rectangular, and triangular lines $S(2 : 1, 1)$, $S(2 : 2, 1)$, $S(2 : 1, 3)$, and $S(2 : 2, 1)$).

between the two modes in Port 1 and Port 2, i.e., $\text{Arg}(S(2 : 1, 1)) - \text{Arg}(S(2 : 2, 1)) = 90^\circ$, and $\text{Arg}(S(2 : 1, 3)) - \text{Arg}(S(2 : 2, 3)) = -90^\circ$. For a LHCP (or RHCP) wave, $\text{Arg}(S(2 : 1, 1)) - \text{Arg}(S(2 : 2, 1)) = 180^\circ$ (or 0°), and $\text{Arg}(S(2 : 1, 3)) - \text{Arg}(S(2 : 2, 3)) = 0^\circ$ (or -180°), thus, only one specific rectangular port outputs power and the other one is isolated.

The transient electric field in Fig. 8 shows that the circular

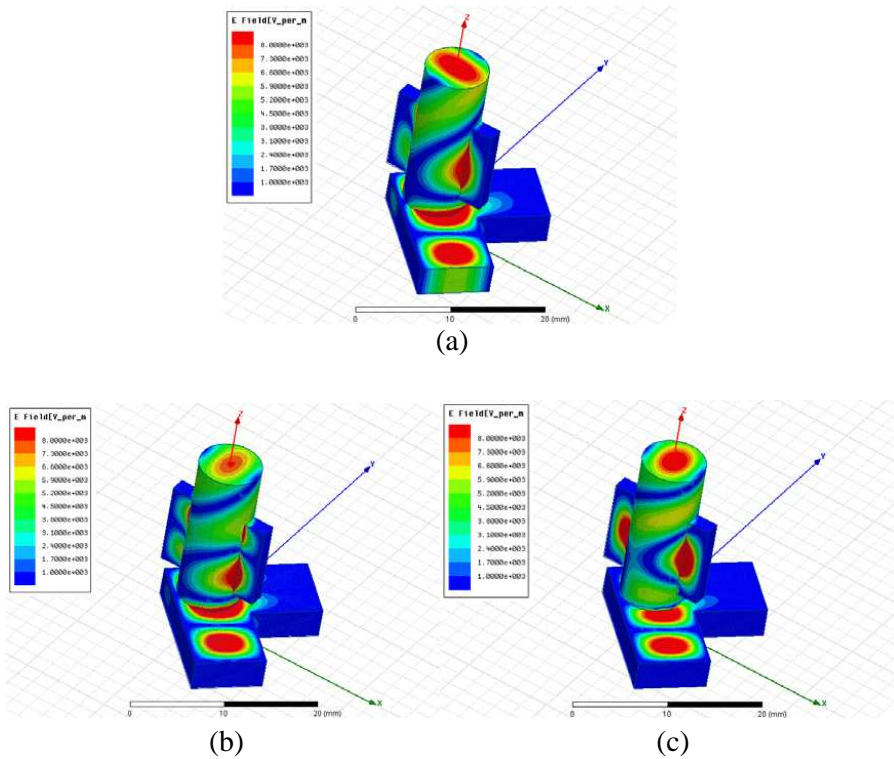


Figure 8. The snapshot electric field on the surface of the circular polarizer; (a) 28 GHz, (b) 31 GHz and (c) 34 GHz.

Table 1. The optimized parameters of the structure (unit in millimeter).

Rectangular waveguide		Circular waveguide	Cylinder Step			
Width	Height	Radius	Radius R_1	Height Z_1	Location X_1	Location Y_2
7.96	3.455	3.5	2.5	1	-0.15	0
Pin				Groove		
Radius R_2	Height Z_2	Location X_2	Location Y_2	height	Depth	Width
0.5	1.3	0.275	0.8	9.85	2.51	1.75

polarized wave from circular waveguide propagates in one rectangular port, and the other rectangular port is isolated. Using only a pair of grooves to realize the broadband circular polarizer has several benefits, including simplification of the design and optimization course, and decreasing the manufacture cost. In addition, this design is suitable for high frequency applications, such as Ka-band and W-band.

A couple of dual circular polarizer with the material of brass have been manufactured, and each includes three pieces: one bottom block, and two top left and right blocks, as illustrated in Fig. 9. The bottom and top blocks are splitted along the centerline of the waveguide, and the circular step and the two pins are located at the bottom block; the top two blocks split the grooves into two equal halves. This compact circular polarizer has an inner volume smaller than $1.5\lambda^3$, and the outer metal block is 1 inch^3 .

Agilent E8364B PNA Network Analyzer is used to measure the S parameters. Two polarizers are connected back to back with a circular waveguide, when two coaxial to WR28 waveguide adapters are used to link the inputs of one polarizer with the PNA, and two Ka-band terminations are combined with the inputs of the other polarizer to measure the return loss and isolation, as shown in Fig. 10(a). The experimental turn loss and isolation is basically consistent with the simulation result, as illustrated in Fig. 11. The bandwidth for return loss $< -15\text{ dB}$ and isolation $< -15\text{ dB}$ is 26%.

When a linear polarizer wave is incident in one rectangular port of the polarizer, a LHCP wave is generated and outputted at the circular port. By placing a short metal plane at the circular port, the polarization of incident LHCP changes to RHCP after reflection,

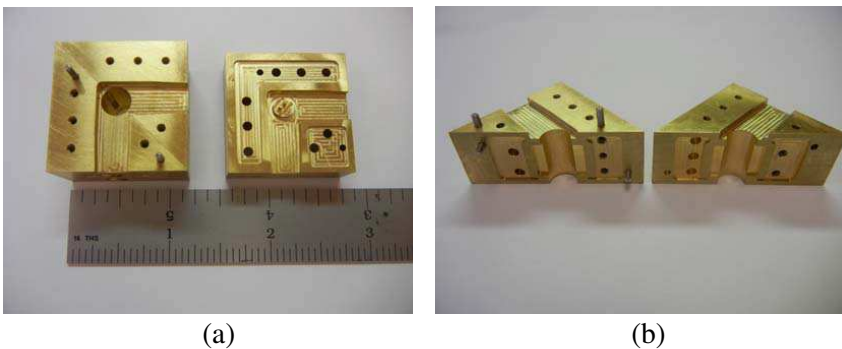


Figure 9. The photographs of split-block design. (a) The top blocks (left) and the upper surface of the bottom block (right); (b) the left and right halves of the top blocks.

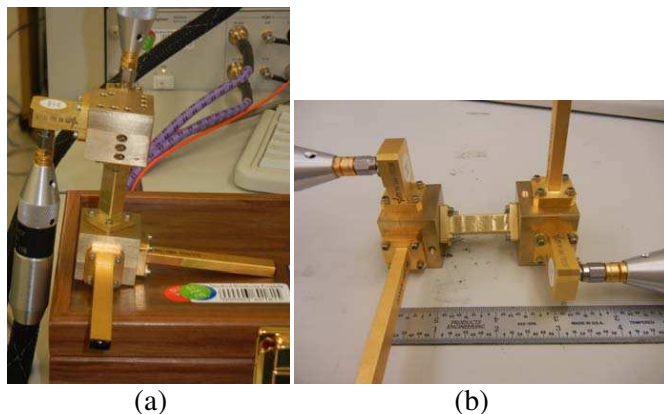


Figure 10. (a) Measurement for return loss and isolation of one polarizer, (b) measurement for circular polarization.

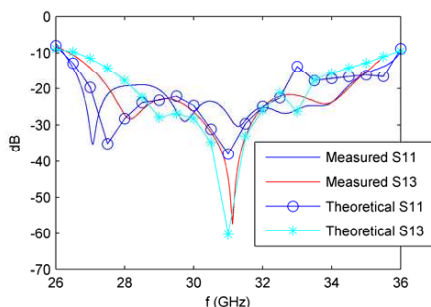


Figure 11. Comparison of the measured and theoretical return loss S_{11} and isolation S_{13} .

thus, the other rectangular port receives the signal, which shows one method to measure the insertion loss of the polarizer [5], as shown in Fig. 12(a). Twice of the averaged insertion loss is about -1.2 dB.

In order to measure the circular polarization, two polarizers are jointed back to back with a circular waveguide, one adapter and one load are connected with one polarizer, as illustrated in Fig. 10(b), the output of the LHCP from one polarizer changes to LP after the second polarizer, and further outputs in one rectangular port, with the other rectangular port isolated. Then, by rotating one of the polarizer successively by 0° , 90° , 180° , and 270° , the outputs of one rectangular port are shown in Fig. 12(b). The axial ratio (AR) of the polarizer shown in Fig. 12(c) means the bandwidth for $AR < 0.5$ dB is about 25%.

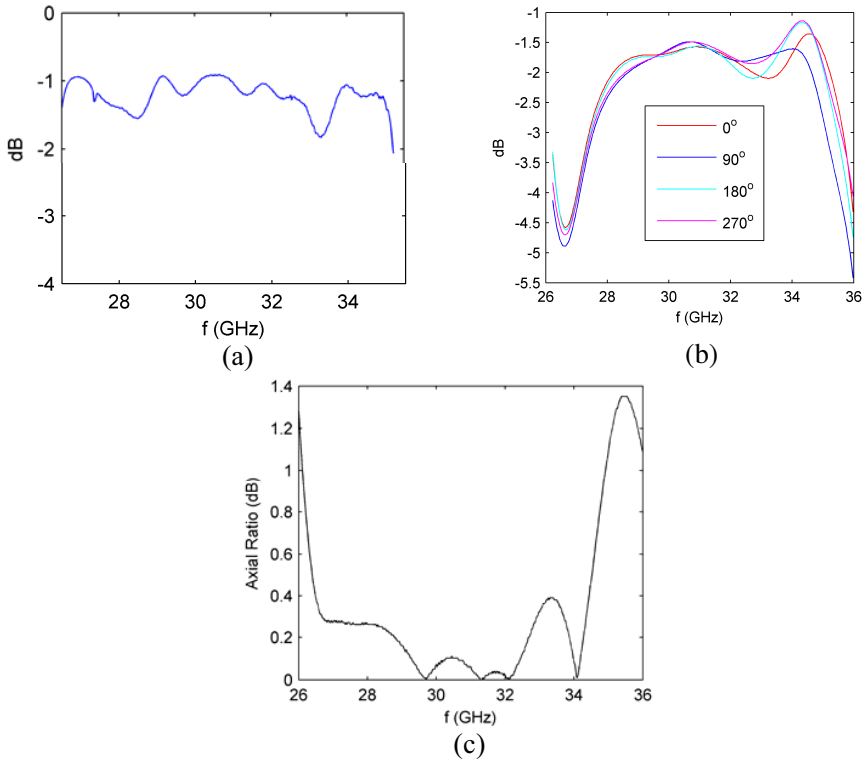


Figure 12. (a) The measured transmission coefficient (twice of the insertion loss) and (b) the output of one rectangular port by successively rotating one polarizer with 0° , 90° , 180° , and 270° and (c) the axial ratio.

Before designing this polarizer, a septum dual circular polarizer at W-band was built, whose performance was not very good with a bandwidth $< 30\%$, and the limited bandwidth maybe came from the non-perfect design. Then, we try to build a more broad-band polarizer, although the bandwidth of the new polarizer is not wider than the septum polarizer.

4. CONCLUSIONS

We present and test a dual circular polarizer that is compact, broadband, and easy to manufacture. The total volume of the polarizing diplexer is smaller than $1.5\lambda^3$ and the bandwidth is about

25%. The design uses simple shapes, so it should be easy to manufacture. Due to the compact size and wide bandwidth, this polarizer can be used in a wide range of applications, including detectors of the CMB.

ACKNOWLEDGMENT

This work is supported by Department of Energy contract DE-AC02-76SF00515.

REFERENCES

1. Kovac, M., E. M. Leitch, C. Pryke, J. E. Carlstrom, N. W. Halverson, and W. L. Holzapfel, "Detection of polarization in the cosmic microwave background using DASI," *Nature*, Vol. 420, 772–787, 2002.
2. QUIET Collaboration, "First season QUIET observations: Measurements of CMB polarization power spectra at 43 GHz in the multipole range $25 \leq \ell \leq 475$," *The Astrophysical Journal*, Vol. 741, No. 2, Article ID 111, 2011.
3. Piovano, B., G. Bertin, L. Accatino, and M. Mongiardo, "CAD and optimization of compact wide-band septum polarizers," *Eur. Microwave Conf.*, Munich, Germany, 1999.
4. Bornemann, J. and V. A. Labay, "Ridge waveguide polarizer with finite and stepped-thickness septum," *IEEE Trans. Microwave Theory Tech.*, Vol. 43, 1782–1787, Aug. 1995.
5. Zhong, W., B. Li, Q. Fan, and Z. Shen, "X-band compact septum polarizer design," *ICMTCE*, 167–170, May 22–25, 2011.
6. Virone, G., R. Tascone, M. Baralis, O. A. Peverini, A. Olivieri, and R. Orta, "A novel design tool for waveguide polarizers," *IEEE Trans. Microwave Theory Tech.*, Vol. 53, No. 3, Part 1, 888–894, Mar. 2005.
7. Yoneda, N., M. Miyazaki, T. Horie, and H. Satou, "Mono-grooved circular waveguide polarizers," *2002 IEEE MTT-S International Microwave Symposium Digest*, Vol. 2, 821–824, 2002.
8. Jung, Y. B., "Ka-band polariser structure and its antenna application," *ETRI J.*, Vol. 45, 931–932, 2009.
9. Eom, S. Y. and Y. B. Korchemkin, "A new comb circular polarizer suitable for millimeter-band application," *ETRI J.*, Vol. 28, No. 5, 656–659, Oct. 2006.
10. Virone, G., R. Tascone, O. A. Peverini, G. Addamo, and

- R. Orta, "Combined-phase-shift waveguide polarizer," *IEEE Microw. Wirel. Compon. Lett.*, Vol. 18, No. 8, 509–511, 2008.
11. Wang, S. W., C. H. Chien, C. L. Wang, and R. B. Wu, "A circular polarizer designed with a dielectric septum loading," *IEEE Trans. Microwave Theory Tech.*, Vol. 52, 1719–1723, Jul. 2, 2004.
 12. Bertin, G., B. Piovano, L. Accatino, and M. Mongiardo, "Full-wave design and optimization of circular waveguide polarizers with elliptical irises," *IEEE Trans. Microw. Theory Tech.*, Vol. 50, No. 4, 1077–1083, Apr. 2002.
 13. Boifot, A. M., "Classification of ortho-mode transducers," *Euro. Trans. Telecommun. and Related Technol.*, Vol. 2, 503–510, 1991.
 14. Aramaki, Y., N. Yoneda, M. Miyazaki, and T. Horie, "Ultra-thin broadband OMT with turnstile junction," *IEEE MTT-S Int. Dig.*, Vol. 1, 47–50, Jun. 2003.
 15. Navarrini, A. and R. L. Plambeck, "A turnstile junction waveguide orthomode transducer," *IEEE Trans. Microw. Theory Tech.*, Vol. 54, No. 1, 272–277, Jan. 2006.
 16. Pisano, G., et al., "A broadband WR10 turnstile junction orthomode transducer," *IEEE Microw. Wirel. Compon. Lett.*, Vol. 17, 286, 2007.
 17. Yoneda, N., M. Miyazaki, and T. Noguchi, "A 90 GHz-band monoblock type waveguide orthomode transducer," *1999 IEEE MTT-S International Microwave Symposium Digest*, Vol. 4, 1781–1784, 1999.
 18. Heidari, A., M. Heyrani, and M. Nakhkash, "A dual-band circularly polarized stub loaded microstrip patch antenna for GPS applications," *Progress In Electromagnetics Research*, Vol. 92, 195–208, 2009.
 19. Wu, G.-L., W. Mu, G. Zhao, and Y.-C. Jiao, "A novel design of dual circularly polarized antenna FED by L-strip," *Progress In Electromagnetics Research*, Vol. 79, 39–46, 2008.
 20. Chen, X., G. Fu, S.-X. Gong, Y.-L. Yan, and J. Chen, "Parametric studies on the circularly polarized stacked annular-ring microstrip antenna," *Progress In Electromagnetics Research C*, Vol. 12, 65–77, 2010.
 21. Lin, C., F.-S. Zhang, Y. Zhu, and F. Zhang, "A novel three-fed microstrip antenna for circular polarization application," *Journal of Electromagnetic Waves and Applications*, Vol. 24, Nos. 11–12, 1511–1520, 2010.
 22. Lai, C.-H., T.-R. Chen, and T.-Y. Han, "Circularly-polarized reconfigurable microstrip antenna," *Journal of Electromagnetic*

- Waves and Applications*, Vol. 23, Nos. 2–3, 195–201, 2009.
23. Masa-Campos, J. L. and F. Gonzalez-Fernandez, “Dual linear/circular polarized planar antenna with low profile double-layer polarizer of 45° tilted metallic strips for WiMAX applications,” *Progress In Electromagnetics Research*, Vol. 98, 221–231, 2009.
 24. Sze, J.-Y. and S.-P. Pan, “Design of broadband circularly polarized square slot antenna with a compact size,” *Progress In Electromagnetics Research*, Vol. 120, 513–533, 2011.
 25. HFSS, USA, <http://www.ansys.com/>